Chapter 3

OPTIMISING THE NUMBER OF DOUBLE-DIFFERENCED OBSERVATIONS FOR GPS NETWORKS IN SUPPORT OF DEFORMATION MONITORING APPLICATIONS

3.1 Introduction

Deformation monitoring using GPS techniques is usually carried out by installing and operating a local network of GPS receivers located on and around the deforming body, e.g. the flanks of a volcano, or on a dam wall, bridge structure, etc. As mentioned in chapter 2, GPS networks for deformation monitoring can generally be observed in two ways, using either episodic campaigns or continuous measurements. Campaign-style surveys are conducted by reoccupying the same stations every few months or so to detect movements between campaigns. While these measurements have produced useful results (e.g. Abidin et al., 1998; Nishi et al., 1999; Shepherd et al., 1998), they give no indication of short-term ground movement in the long periods between the campaigns. Continuous GPS networks, however, can potentially monitor all ground deformation signals and thus give detailed information about the dynamics of the deforming body.

As described in section 2.5.3, different data processing strategies can be used depending on the type of deformation expected. If 'slow' deformation at a constant rate (with time) is expected (e.g. tectonic plate movement or ground subsidence), the data is usually processed in static sessions of a few hours to a few days in length. A comparison of several annually or quarterly conducted GPS campaigns is normally sufficient to derive the average rate of deformation in such cases. If the deformational signal is expected to occur over a short period of time ('sudden' deformation, e.g. caused by earthquakes) and/or varies with time ('fast' continuous deformation, e.g. long suspension bridges), the sampling interval needs to be increased to track these motions. If the deformation can cause failure of the deforming body (e.g. a collapsing dam or bridge, or an erupting volcano), a (near) real-time, epoch-by-epoch solution is desired in order to detect the deformation as soon as it occurs, and so as to initiate warning and evacuation procedures.

In the case of volcano deformation monitoring, the movements are expected to be of a mixed nature. While the deformation will be slow or even negligible during periods of quiescence, increased activity before an eruption will cause changing ground movement rates due to the expansion of the magma chamber below the volcano. A real-time, epoch-by-epoch solution is therefore preferable in order to detect movements on the flanks of a volcano with minimum delay. However, one has to keep in mind that a decreasing observation period increases the difficulty in resolving integer phase ambiguities. Hence, there is a trade-off between the length of the observation period and the difficulty in computing a reliable solution (see Roberts, 2002).

Multi-baseline processing strategies are preferred because all baselines are then computed together, taking into account the between-baseline correlations which arise from observing a GPS network simultaneously. Commercial software packages use a baseline-by-baseline processing approach, and therefore neglect these correlations (see section 3.4). Note, however, that some scientific software packages are able to use a different number of satellites for different baselines. GAMIT, for instance, uses all available double-differenced observations and accounts for this by using appropriate variances in the data processing (King & Bock, 1995). The Bernese software, on the other hand, scans all possible baselines first and then selects an independent set of double-differences, generally based on the shortest baselines (Rothacher & Mervart, 1996).

For the volcano deformation monitoring application there is a special challenge. The sides of the volcano will block out part of the sky, and therefore the network of receivers is not likely to track many satellites that are visible from all receivers simultaneously. Figure 3.1 shows the typical terrain consideration around a volcano. A GPS receiver on the summit would have a clear skyview but would be in great danger of being damaged by emission of gas and material, especially during periods of volcanic activity. Therefore the monitoring receivers are generally placed on the flanks of the volcano. If the usual base-station / base-satellite approach is used in the multi-baseline data processing, only the common satellites are considered, resulting in the total number of possible double-differences being comparatively low, hence a lot of valuable information can be lost. In the worst case, a solution may not be obtained if the number of common satellites tracked

by all network receivers is reduced to less than four. In this chapter a method is described that considers satellites that are visible from a small number of GPS network stations only. Hence, the number of independent double-differenced observables can be maximised, which in turn would permit a more precise and reliable solution.

Fig. 3.1: Gunung Merapi, Indonesia

3.2 Generating an Independent Set of Double-Differences

When processing data from a local GPS network, double-differenced observables between pairs of receivers and pairs of satellites are used, rather than raw 'one-way' carrier phase measurements. The double-differences constructed from phase measurements made by two receivers m and n to two satellites i and j eliminate the two receiver clock biases and the two satellite clock biases (e.g. Hofmann-Wellenhof et al., 2001; Rizos, 1997):

$$\phi_{mn}^{ij} = \phi_n^j - \phi_n^i - \phi_m^j + \phi_m^i \qquad (3\text{-}1)$$

ϕ_m^i denotes the 'one-way' carrier phase measurement between receiver m and satellite i.

In general, considering a network of r receivers tracking s satellites, the number of possible double-differences that can be formed is:

$$n_{DD} = \binom{s}{r} = \frac{s \cdot (s-1) \cdot (s-2) \cdot \ldots \cdot (s-r+1)}{1 \cdot 2 \cdot 3 \cdot \ldots \cdot r} \tag{3-2}$$

However, only (r-1)·(s-1) of these double-differences are *linearly independent*. Hence any additional double-difference can be formed as a linear combination of the independent set of double-differences. These linearly dependent double-differences do not add any new information to the least squares data processing, and in fact artificially increase the redundancy, which is not desired. Usually the common satellites visible from all network GPS receivers are determined and a 'base station' and a 'base satellite' are selected to generate such an independent set of double-differenced observables.

Consider, for instance, two sites, both tracking the same seven satellites. If one of the receivers is selected as the 'base station' (say m = 1) and one of the satellites is selected as the 'base satellite' (say i = 1), six double-differenced observables ϕ_{12}^{1j} with j = 2, 3, …, 7 can be formed according to equation (3-1). However, this is not the only scheme available to obtain a set of independent double-differences. Another frequently used method is referred to as *sequential* double-differencing. Instead of using a 'base satellite' the satellites are sorted in ascending order and the double-differenced observable is formed between pairs of sequential satellites, in this example resulting in ϕ_{12}^{ij} with (i,j) = {(1,2), (2,3), …, (6,7)}. The situation becomes more complex when the network receivers each track some, but not all, of the satellites, as is likely in a local network around a volcano. The problem becomes apparent by expanding the previous example to three GPS network receivers each tracking some of the seven satellites, but with only three common satellites visible from all sites. If the usual base-station / base-satellite approach is used, only four double-differences can be formed in this case – not enough to obtain a coordinate solution for the two 'rover' sites. However, if satellites that are only visible by two of the three receivers were considered in the data processing, the number of double-differenced observables could be increased.

The data processing approach described here determines the receiver-to-satellite connections for each site of the network. A maximum set of independent double-differenced combinations is computed using vector space methods, and the geometric characterisations of Boolean matrices, as suggested by Saalfeld (1999). Hence, by using

all the available information, the number of independent double-differenced observables can be optimised, permitting a more precise and reliable solution.

The Saalfeld (1999) algorithm uses a Boolean matrix of zeroes and ones to represent the receiver-to-satellite connections, where a 1 denotes that a certain satellite can be viewed by a certain network receiver. If this *connection matrix* is built so that the receivers are arranged in rows and the satellites are arranged in columns, an axis-parallel rectangle of 1s will represent a possible double-difference (Fig. 3.2).

	S_1	S_2	S_3	S_4	S_5	S_6	S_7	S_8	S_9
R_1	1	0	1	1	1	1	1	1	1
R_2	1	1	1	1	0	1	1	1	1
R_3	0	1	1	1	1	1	0	1	1
R_4	1	0	1	1	1	0	1	1	1
R_5	1	1	1	0	1	0	1	1	1
R_6	1	0	1	1	0	1	0	1	1

Fig. 3.2: Sample receiver-to-satellite connection matrix for 6 receivers and 9 satellites

For example, in Figure 3.2, a possible combination using receivers R_1 and R_2 and satellites S_3 and S_6 results in the double-differenced phase observable:

$$\phi_{12}^{36} = \phi_2^6 - \phi_2^3 - \phi_1^6 + \phi_1^3 \qquad (3\text{-}3)$$

On the other hand, receivers R_1 and R_2 cannot form a double-difference with satellites S_2 and S_3. Some of the rectangles can be formed by appending or subtracting two other rectangles that share a common side. These newly formed rectangles correspond to linearly dependent double-differences. In Figure 3.2, the above mentioned double-difference can also be obtained by a linear combination of two other double-differences, e.g.

$$\phi_{12}^{36} = \phi_{12}^{34} + \phi_{12}^{46} \qquad \text{or} \qquad \phi_{12}^{36} = \phi_{12}^{16} - \phi_{12}^{13} \; . \qquad (3\text{-}4)$$

The connection matrix is processed by rows, and within each row by columns. For each element containing a 1, the *submatrix* having this element in the lower-right corner is formed. Figure 3.3 shows the submatrix of connection matrix element a_{57}, which

represents the connection between receiver R_5 and satellite S_7. The size of the submatrix is then reduced by removing all rows for which $a_{i7} = 0$ and all columns for which $a_{5j} = 0$, resulting in the *reduced submatrix* shown in Figure 3.4. The size of this submatrix is then further reduced by also removing the row corresponding to R_5 and the column referring to S_7. Thus, a matrix representing the possible upper-left corners of the rectangles having element a_{57} in their lower-right corner is created (Fig. 3.5). This matrix is referred to as the *upper-left corner matrix* and is used to identify the set of independent double-differences.

	S_1	S_2	S_3	S_4	S_5	S_6	S_7
R_1	1	0	1	1	1	1	1
R_2	1	1	1	1	0	1	1
R_3	0	1	1	1	1	1	0
R_4	1	0	1	1	1	0	1
R_5	1	1	1	0	1	0	1

Fig. 3.3: Submatrix of connection matrix element a_{57}

	S_1	S_2	S_3	S_5	S_7
R_1	1	0	1	1	1
R_2	1	1	1	0	1
R_4	1	0	1	1	1
R_5	1	1	1	1	1

Fig. 3.4: Reduced submatrix of connection matrix element a_{57}

	S_1	S_2	S_3	S_5
R_1	1	0	1	1
R_2	1	1	1	0
R_4	1	0	1	1

Fig. 3.5: Upper-left corner matrix of connection matrix element a_{57}

Two non-zero entries of the upper-left corner matrix are *path-connected* if there exists a sequence of 1s between them where successive elements are either in the same row or in the same column. The path-connected components in the upper-left corner matrix each consist of all the non-zero entries in a union of rows (or columns) of this matrix. Hence, whole rows either participate completely in the path-connected component or have no 1s intersecting the component. Two 1s in the upper-left corner matrix correspond to linear

dependent double-differences if and only if they are in the same path-connected component. Hence, by finding all path-connected components of the upper-left corner matrix, and selecting a representative from each, the independent set of double-differences can be obtained. Note that this set no longer refers to just one base station and one specific base satellite.

In this example, Figure 3.5 contains only one path-connected component. If the upper-left most non-zero entry is selected as a representative, the resulting double-difference obtained here is ϕ_{15}^{17}. If the entire receiver-to-satellite connection matrix shown in Figure 3.2 is processed in such manner, the following set of 29 independent double-differences is generated:

$$\phi_{12}^{13},\ \phi_{12}^{14},\ \phi_{12}^{16},\ \phi_{12}^{17},\ \phi_{12}^{18},\ \phi_{12}^{19},\ \phi_{23}^{23},\ \phi_{13}^{34},\ \phi_{13}^{35},\ \phi_{13}^{36},\ \phi_{13}^{38},\ \phi_{13}^{39},\ \phi_{14}^{13},\ \phi_{34}^{14},$$
$$\phi_{14}^{15},\ \phi_{14}^{17},\ \phi_{14}^{18},\ \phi_{14}^{19},\ \phi_{25}^{12},\ \phi_{15}^{13},\ \phi_{15}^{17},\ \phi_{15}^{17},\ \phi_{15}^{18},\ \phi_{15}^{19},\ \phi_{16}^{13},\ \phi_{16}^{14},\ \phi_{16}^{16},\ \phi_{16}^{18},\ \phi_{16}^{19}.$$

Further details of the algorithm can be found in Saalfeld (1999).

3.3 Optimising the Double-Differencing Operator

The set of independent double-differences is used to construct the optimised double-differencing operator that transforms the one-way carrier phase measurements into independent double-differenced observables. This double-differencing operator will take into account all available information. If D denotes the double-differencing operator and Φ denotes the vector of one-way (satellite-to-receiver) carrier phase measurements, the vector of double-differences Φ_D is:

$$\Phi_D = D \cdot \Phi \tag{3-5}$$

In the example presented in Figure 3.2, assume a sub-network of three GPS receivers tracking seven satellites. The receiver-to-satellite connection matrix for this sub-network is shown in Figure 3.6.

	S_1	S_2	S_3	S_4	S_5	S_6	S_7
R_1	1	0	1	1	1	1	1
R_2	1	1	1	1	0	1	1
R_3	1	1	1	1	1	1	0

Fig. 3.6: Sample receiver-to-satellite connections for 3 receivers and 7 satellites

In commercial software, using the conventional data processing approach of one base station and one base satellite, only the common satellites are used to compute a solution. In this example, using R_1 as base station and S_1 as the base satellite, this approach results in six independent double-differences:

ϕ_{12}^{13}, ϕ_{12}^{14}, ϕ_{12}^{16}, ϕ_{13}^{13}, ϕ_{13}^{14}, and ϕ_{13}^{16}.

The resulting double-differencing operator D_{conv} has the form:

$$D_{conv} = \begin{bmatrix} 1 & -1 & 0 & 0 & -1 & 1 & 0 & 0 & 0 & 0 & 0 & 0 \\ 1 & 0 & -1 & 0 & -1 & 0 & 1 & 0 & 0 & 0 & 0 & 0 \\ 1 & 0 & 0 & -1 & -1 & 0 & 0 & 1 & 0 & 0 & 0 & 0 \\ 1 & -1 & 0 & 0 & 0 & 0 & 0 & 0 & -1 & 1 & 0 & 0 \\ 1 & 0 & -1 & 0 & 0 & 0 & 0 & 0 & -1 & 0 & 1 & 0 \\ 1 & 0 & 0 & -1 & 0 & 0 & 0 & 0 & -1 & 0 & 0 & 1 \end{bmatrix} \quad (3\text{-}6)$$

Each row corresponds to a double-difference, and each column represents a particular satellite (in this case S_1, S_3, S_4, and S_6). The first four columns are related to receiver R_1, while columns 5-8 and 9-12 refer to R_2 and R_3 respectively. The positions of the –1s, 0s and 1s within the matrix originate from the construction of a specific double-difference according to equation (3-1).

The alternative approach takes all available information into account resulting in nine double-differenced observables:

ϕ_{12}^{13}, ϕ_{12}^{14}, ϕ_{12}^{16}, ϕ_{12}^{17}, ϕ_{23}^{12}, ϕ_{13}^{13}, ϕ_{13}^{14}, ϕ_{13}^{15}, and ϕ_{13}^{16}.

The optimised double-differencing operator D_{opt} in this case is:

$$D_{opt} = \begin{bmatrix} 1 & 0 & -1 & 0 & 0 & 0 & 0 & -1 & 0 & 1 & 0 & 0 & 0 & 0 & 0 & 0 & 0 & 0 & 0 & 0 & 0 \\ 1 & 0 & 0 & -1 & 0 & 0 & 0 & -1 & 0 & 0 & 1 & 0 & 0 & 0 & 0 & 0 & 0 & 0 & 0 & 0 & 0 \\ 1 & 0 & 0 & 0 & 0 & -1 & 0 & -1 & 0 & 0 & 0 & 0 & 1 & 0 & 0 & 0 & 0 & 0 & 0 & 0 & 0 \\ 1 & 0 & 0 & 0 & 0 & 0 & -1 & -1 & 0 & 0 & 0 & 0 & 0 & 1 & 0 & 0 & 0 & 0 & 0 & 0 & 0 \\ 0 & 0 & 0 & 0 & 0 & 0 & 0 & 1 & -1 & 0 & 0 & 0 & 0 & 0 & -1 & 1 & 0 & 0 & 0 & 0 & 0 \\ 1 & 0 & -1 & 0 & 0 & 0 & 0 & 0 & 0 & 0 & 0 & 0 & 0 & 0 & -1 & 0 & 1 & 0 & 0 & 0 & 0 \\ 1 & 0 & 0 & -1 & 0 & 0 & 0 & 0 & 0 & 0 & 0 & 0 & 0 & 0 & -1 & 0 & 0 & 1 & 0 & 0 & 0 \\ 1 & 0 & 0 & 0 & -1 & 0 & 0 & 0 & 0 & 0 & 0 & 0 & 0 & 0 & -1 & 0 & 0 & 0 & 1 & 0 & 0 \\ 1 & 0 & 0 & 0 & 0 & -1 & 0 & 0 & 0 & 0 & 0 & 0 & 0 & 0 & -1 & 0 & 0 & 0 & 0 & 1 & 0 \end{bmatrix} \quad (3\text{-}7)$$

Obviously the optimised double-differencing operator matrix is of larger dimension than the conventional operator matrix because it considers all seven satellites in view across the network. The first seven columns relate these satellites to R_1, while columns 8-14 and 15-21 refer to R_2 and R_3 respectively.

Using a double-differencing operator in the multi-baseline data processing is one of the most efficient means of taking into account the between-baseline correlations (Craymer & Beck, 1992). This is discussed further in the next section.

3.4 Multi-Baseline Processing versus Baseline-By-Baseline Processing

Data collected by a network of GPS receivers can be processed essentially in two ways: (a) the multi-baseline mode, or (b) the single-baseline mode. Only the multi-baseline approach is rigorously correct because between-baseline correlations introduced by observing the baselines simultaneously are considered. However, most available commercial software are only capable of processing data in the single-baseline mode.

In the baseline-by-baseline approach, the data processing is done in two steps. First the single baseline solution vectors are obtained (neglecting the between-baseline correlations). These are then used as input for the second step, the network adjustment used to derive the final station coordinates. Normally a set of independent baseline solutions is selected for the network adjustment. Consider, for example, a network of four GPS sites denoted A, B, C and D. One possible set of independent baselines is AB, BC and CD; another consists of the baselines AB, AC and AD. However, the final coordinate results will be different, depending on which set of independent baselines is

chosen. Hence the coordinate solution is not unique. Usually the shortest baselines are selected in order to reduce the impact of the unmodelled atmospheric biases.

Han & Rizos (1995) describe a methodology for obtaining more reliable results by processing all possible baselines in the single-baseline mode. In the subsequent network adjustment the baselines' co-factor matrices are scaled by r/2 (r being the number of network receivers) to account for the fact that all baselines are processed. However, this procedure is suitable only for exactly simultaneous sessions, i.e. all receivers commencing and stopping data collection at the same time. Moreover, the assumption of identical design matrices for all sites is only valid for small networks with baseline lengths of up to 20km. Ibid (1995) state that if outliers are present in the double-differenced data and are deleted during a baseline solution, the data for the same time interval should also be deleted for all other baseline determinations. This will lead to 'good' data (collected on baselines not affected by outliers) being discarded in the processing.

In multi-baseline mode the data processing is performed in one step. A double-differencing operator is formed for the whole network, resulting in a fully populated co-factor matrix that accounts for the between-baseline correlations. Also a stochastic model for double-differences is used. Applying the error-propagation law, the resulting co-factor matrix C_M is obtained by:

$$C_M = D_M \cdot C_\phi \cdot D_M{}^T \tag{3-8}$$

C_ϕ denotes the variance-covariance matrix of the raw carrier phase observations and D_M denotes the double-differencing operator. C_ϕ is a diagonal block matrix containing the a priori variances of the phase observations. The co-factor matrix C_M is fully populated, and the resulting coordinates are the same no matter which set of independent double-differences is selected.

The situation can be illustrated by referring to the earlier example. In a network of four GPS receivers A, B, C and D, three independent baselines AB, AC and AD can be formed with A being selected as the reference site. Let all receivers track the same four

satellites and assume, for the sake of simplicity, the same variance σ^2 for all carrier phase observations from the receivers to the satellites. The variance-covariance matrix

$$C_\phi = \text{diag}\,(\sigma^2) \tag{3-9}$$

has the dimension [r·s, r·s], r being the number of receivers and s denoting the number of satellites. In the baseline-by-baseline approach the three baselines are computed one after the other, resulting in a C_ϕ of dimension [8, 8]. Following equation (3-8), the co-factor matrices C_S for the single-baseline mode can be derived:

$$C_S^{AB} = C_S^{AC} = C_S^{AD} = \begin{bmatrix} 4s^2 & 2s^2 & 2s^2 \\ 2s^2 & 4s^2 & 2s^2 \\ 2s^2 & 2s^2 & 4s^2 \end{bmatrix} \tag{3-10}$$

Due to the assumptions made above, C_S is identical for the three baselines. In multi-baseline mode the baselines are processed together resulting in the co-factor matrix C_M:

$$C_M = \begin{bmatrix} C_S^{AB} & C_{AC}^{AB} & C_{AD}^{AB} \\ C_{AC}^{AB} & C_S^{AC} & C_{AD}^{AC} \\ C_{AD}^{AB} & C_{AD}^{AC} & C_S^{AD} \end{bmatrix} \tag{3-11a}$$

where

$$C_{AC}^{AB} = C_{AD}^{AB} = C_{AD}^{AC} = \begin{bmatrix} 2s^2 & s^2 & s^2 \\ s^2 & 2s^2 & s^2 \\ s^2 & s^2 & 2s^2 \end{bmatrix} \tag{3-11b}$$

The matrix C_{AC}^{AB} describes the correlation between the baselines AB and AC, which is neglected in the baseline-by-baseline solution. The matrices C_{AD}^{AB} and C_{AD}^{AC} have a similar structure. Figure 3.7 shows the general structure of the block matrix C_M for a network of four receivers. Note that all the correlations would be set to zero in single-baseline processing.

Baseline 1	Correlation 1-2	Correlation 1-3
Correlation 1-2	Baseline 2	Correlation 2-3
Correlation 1-3	Correlation 2-3	Baseline 3

Fig. 3.7: Structure of the resulting co-factor matrix C_M in multi-baseline mode

The effect of these correlations on GPS network computation was investigated by Santos et al. (1997). It was shown that by taking the between-baseline correlations into account, improved baseline results and more realistic precisions of the estimated baseline components can be obtained.

3.5 Ambiguity Resolution

In order to detect deformational signals over a short period of time, it is desired to compute a solution with minimum delay. Ideally, a coordinate set should be available each measurement epoch, effectively operating in a 'kinematic' mode of positioning. However, due to the nature of the carrier phase observations, the initially unknown integer ambiguities have to be resolved first. This process becomes increasingly difficult with decreasing observation session length, and is therefore a considerable challenge for single-epoch solutions unless the process is somehow aided. (Note that cycle slips do not have to be considered in an epoch-by-epoch solution such as this.)

Single-epoch solutions are desirable for deformation monitoring of hazardous structures such as volcanoes because they potentially produce near-real-time information about GPS baseline changes. Appropriate analysis of the time series of coordinate solutions enables authorities to put into effect plans that mitigate the impact of an eruption. Moreover, short-term movements can be picked up and used to better understand the dynamics of the deforming body. Solutions produced every few hours, or on a daily basis, will not be able to provide such detailed information. However, decreasing the observation period causes difficulties in 'fixing' the ambiguities to integer values. As the initial carrier phase ambiguity is constant as long as the receiver maintains lock on the satellite, the probability of its correct determination will increase with changing satellite geometry over time. Hence, ambiguity resolution can prove to be extremely difficult for single-epoch solutions, if no a priori information is available.

The basic approach to determining the integer ambiguities is to use the relatively noisy pseudorange measurements to define a search volume, which is assumed to contain the correct set of integer ambiguities. All possible integer ambiguity combinations are then tested to determine the best set, the test criterion often being the ambiguity set that minimises the sum of the squared double-differenced carrier phase residuals. A ratio test is performed between the sum of the squared carrier phase residuals of the 'best' and 'second best' sets, and if the ratio exceeds a certain threshold, then the 'best' set is accepted for fixing the carrier phase ambiguities. Han & Rizos (1996c) have identified six classes of ambiguity resolution (AR) techniques:

- AR using special operational modes, such as 'antenna swap' initialisation, re-occupation procedures, 'stop & go' and relative positioning of a single receiver (Remondi, 1988; Han & Rizos, 1996a).
- AR through a search in the 'Observation Domain', using pseudorange and carrier phase data based on linear combinations of the L1 and L2 carrier phase (with longer wavelength), and/or linear combinations of the L1 and L2 P-code pseudorange (with lower noise) (Han & Rizos, 1996c).
- AR through a search in the 'Coordinate Domain', such as in the case of the Ambiguity Function Method (AFM) (Remondi, 1989), which requires the use of accurate initial coordinates.
- AR through a search in the 'Estimated Ambiguity Domain' by first estimating the ambiguities as real-valued parameters, and then determining the likeliest integer ambiguities in a least squares estimation process. Examples include the Fast Ambiguity Resolution Approach (FARA) (Frei & Beutler, 1990), the Least Squares Ambiguity Search Technique (LSAST) (Hatch, 1990), the Cholesky Decomposition Method (Euler & Landau, 1992), the Fast Ambiguity Search Filter (FASF) (Chen, 1993) and the Least-squares Ambiguity Decorrelation Adjustment (LAMBDA) (Teunissen, 1995).
- The 'Ambiguity Recovery' technique, where the ambiguity search procedure is based on cycle slip estimation techniques (Han, 1995).
- The 'Integrated Method', which combines the techniques mentioned above, possibly with the addition of other physical sensors such as an Inertial Navigation System (INS), to aid ambiguity resolution (Abidin, 1993; Han & Rizos, 1996b).

Which AR technique is to be used generally depends on the application. The observation mode (e.g. static or kinematic positioning), the length of the observed baselines, the duration of the observation session and the processing mode (e.g. real-time processing or post-processing) all play a role in defining the optimal AR technique. In this case the AR search in the 'Estimated Ambiguity Domain' is adopted in a simplified form. First real-valued ambiguities are determined, which are then simply 'rounded-off' to integers in a second step. This is feasible if the real-valued ambiguity estimates are close to integer values, which is likely to be the case if accurate initial coordinates are available.

It is possible to use high accuracy initial coordinates (± 5cm) in order to aid the resolution of the carrier phase ambiguities on an epoch-by-epoch basis. The initial coordinates are typically obtained from the previous epoch's solution and can provide additional information for the parameter estimation. Hence they are introduced into the least squares process as fictitious 'observations' with their variance-covariance matrix (see equation 3-17). This procedure is suitable for the type of motion expected to occur on an active volcano. While, in times of increased activity, the ground deformation may be rather large, it will occur in a continuous manner. The volcano will not show any sudden 'jumps' between successive measurement epochs (generally 15 or 30 seconds apart).

The variance-covariance matrix C_ϕ used in the data processing contains a priori information about the precision of the observations. It can be used to increase the weight of 'good' observations in comparison to 'bad' observations (the weight matrix being the inverse of the variance-covariance matrix). This is particularly important if different types of geodetic measurements (e.g. GPS and spirit levelling or EDM) are combined in a least squares adjustment. For GPS networks it is often assumed that all observations taken between the network sites and the orbiting satellites are independent and of equal quality, resulting in the same diagonal matrix of equal variances for each GPS receiver (equation 3-9). In this case, however, a specific variance-covariance matrix C_{ϕ_i} is computed for each receiver i based on the elevation of the observed satellites, rather than assuming that the conditions at all network sites are the same. Hence, the resulting variance-covariance

matrix C_ϕ for the whole network is a diagonal block matrix consisting of *different* C_{ϕ_i} matrices (r and s denoting the number of receivers and satellites, respectively):

$$C_\phi = \begin{bmatrix} C_{\phi_1} & 0 & \cdots & 0 \\ 0 & C_{\phi_2} & \cdots & 0 \\ \vdots & \vdots & \ddots & \vdots \\ 0 & 0 & \cdots & C_{\phi_r} \end{bmatrix} \tag{3-12a}$$

where

$$C_{\phi_i} = \begin{bmatrix} (\sigma_i^1)^2 & 0 & \cdots & 0 \\ 0 & (\sigma_i^2)^2 & \cdots & 0 \\ \vdots & \vdots & \ddots & \vdots \\ 0 & 0 & \cdots & (\sigma_i^s)^2 \end{bmatrix} \tag{3-12b}$$

It is well known that most of the residual unmodelled biases are dependent on the satellite elevation. An exponential function can be used to represent the standard deviation of the one-way L1 observations for satellite j (Han, 1997):

$$\sigma^j = s \cdot \left(a_0 + a_1 \cdot \exp(-E^j / E_0) \right) \tag{3-13}$$

where σ^j is the standard deviation of the L1 observations for satellite j with elevation angle E^j. The s represents a scale factor. The values for a_0, a_1 and E_0 are approximated by constants, which can be empirically determined. Table 3.1 shows the values for L1 carrier phase observations, obtained by Ibid (1997), which are used in the UNSW-designed baseline processing software. The corresponding values for pseudorange observations are also given.

Tab. 3.1: Standard deviation of one-way L1 observations

	a_0 [m]	a_1 [m]	E_0 [°]
Carrier phase observations	0.003	0.026	20
Pseudorange observations	0.070	0.600	20

In the usual least squares procedure the unknown parameter correction vector δX is determined using the equations (e.g. Harvey, 1994; Koch, 1999):

$$V = A \cdot \delta X_0 - L \tag{3-14}$$

$$\delta X = (A^T P A)^{-1} A^T P L \tag{3-15}$$

where V = error vector
A = design matrix
δX_0 = vector of initial coordinates
L = observation vector
P = weight matrix

The root mean square is:

$$RMS = \sqrt{\frac{V^T P V}{n - u}} \tag{3-16}$$

where n = number of observations
u = number of unknowns

If the initial coordinates X_0 are introduced as 'observations' with their variance-covariance matrix D_X, which is equivalent to the Bayesian least squares approach (see Koch, 1990), the equations are as follows (Kleusberg & Teunissen, 1996; Vaníček & Krakiwsky, 1986):

$$\delta X = (A^T P A + D_X^{-1})^{-1} A^T P L \tag{3-17}$$

$$RMS = \sqrt{\frac{V^T P V + \delta X^T D_X^{-1} \delta X}{(n + u) - u}} = \sqrt{\frac{V^T P V + \delta X^T D_X^{-1} \delta X}{n}} \tag{3-18}$$

3.6 Numerical Example

Data collected from a network of six GPS receivers in Sydney, Australia, with baseline lengths ranging from 2.0 to 2.7km were used to test the data processing procedure. Figure 3.8 shows the location of the network sites, which were carefully chosen to ensure a clear skyview. A 2-hour session was observed on October 12, 1999 using Leica CRS1000 receivers, equipped with choke ring antennas to minimise the effect of multipath. The sampling rate was set to 30 seconds, with a satellite elevation mask angle of 15°.

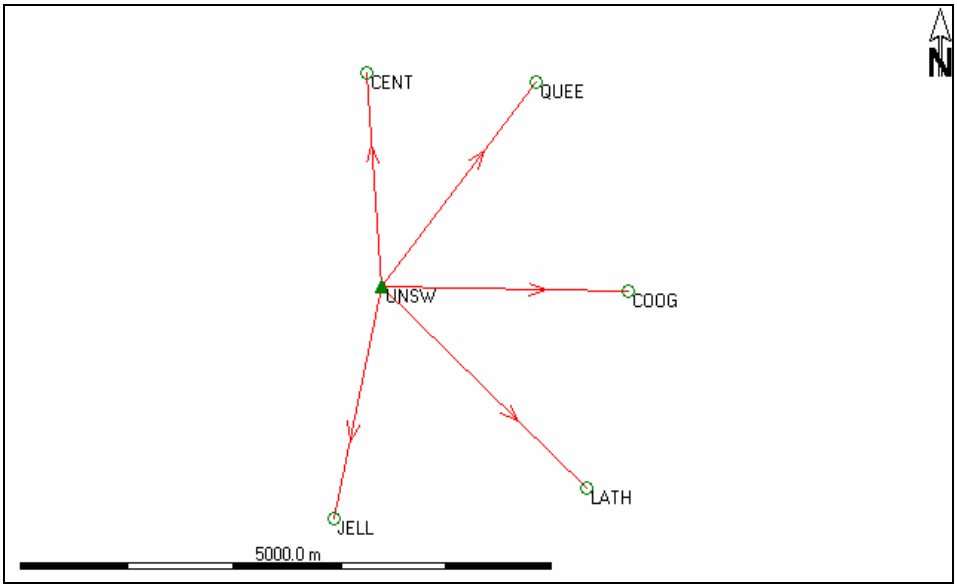

Fig. 3.8: GPS test network at UNSW

The coordinate results obtained from the processing of the 2-hour session were used as the 'true' coordinates against which the single-epoch solutions were compared. The data set was then altered by manually editing data at the network stations. At each site a different azimuth band of 40° pointing towards the centre of the network, with satellite elevations of less than 50°, was blocked out in order to simulate the situation around a volcano. The results of the epoch-by-epoch solution using conventional double-differencing and the proposed approach were compared.

Using the proposed approach, the number of double-differenced observables at each epoch was increased by an average of 9.8 observables, with a maximum difference between the approaches being 20 observations (Fig. 3.9). The minimum number of independent double-differenced observables required to obtain a solution for a network

of six sites is 15. For certain epochs no solution could be obtained using the conventional approach because the number of common satellites tracked by all network receivers dropped to three, resulting in only 10 double-differenced observables. However, using the proposed double-differencing approach satisfactory solutions could be obtained for these epochs.

Figure 3.9 also shows the root mean square of the double-differenced residuals. While the RMS for the proposed method is often slightly higher than for the common method, it shows less variation. The standard deviation of the root mean square was reduced by 34%, from 0.1232m to 0.0811m.

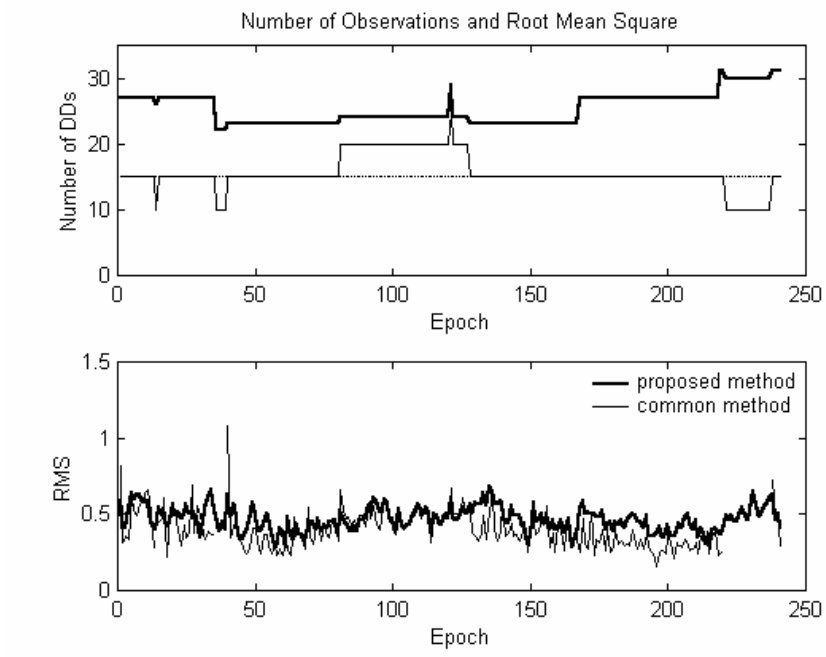

Fig. 3.9: Number of double-differenced observations and RMS of epoch-by-epoch solutions

The coordinates obtained by both data processing approaches were compared against the 'true' coordinate values. Figures 3.10a-e show the resulting coordinate differences. Note that the gaps in the curves representing the 'common satellite method' are caused by an insufficient number of double-differenced observables for those epochs. It can be seen that the proposed method increases the quality of the results. The coordinate variations obtained using the proposed method are also smaller. This can be verified from the standard deviations of the X-, Y- and Z-components shown in Figures 3.11a-e.

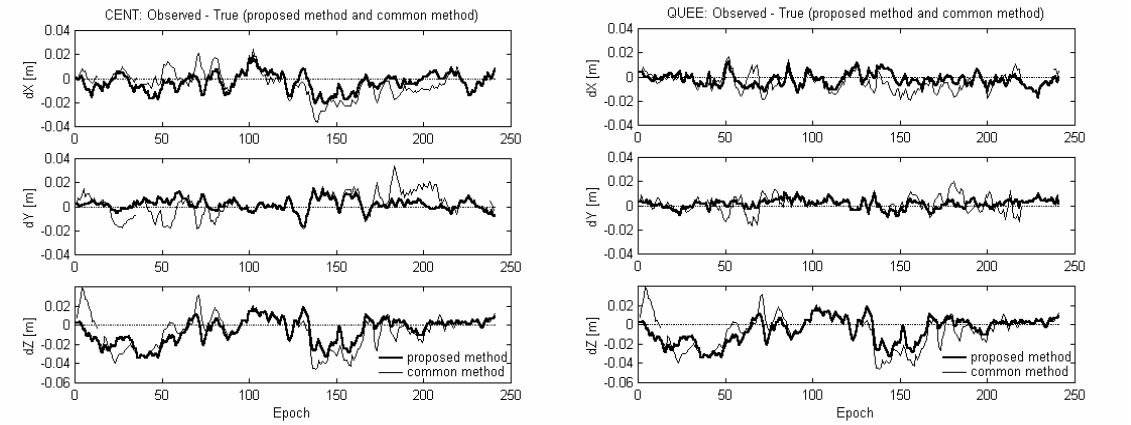

Fig. 3.10a+b: Solution coordinates compared to 'truth' (left: CENT, right: QUEE)

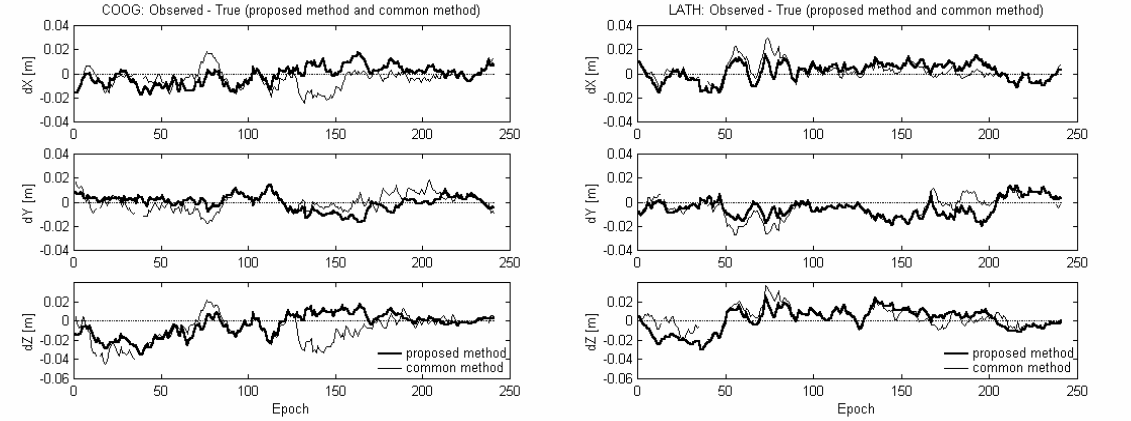

Fig. 3.10c+d: Solution coordinates compared to 'truth' (left: COOG, right: LATH)

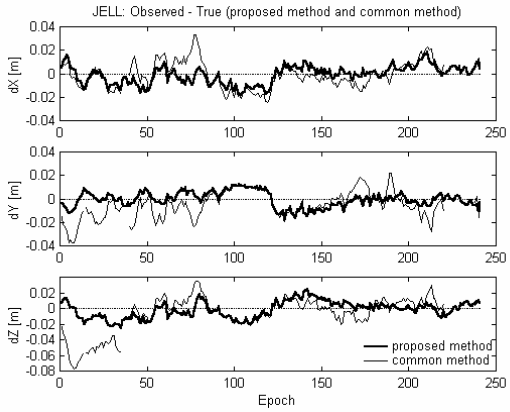

Fig. 3.10e: Solution coordinates compared to 'truth' (JELL)

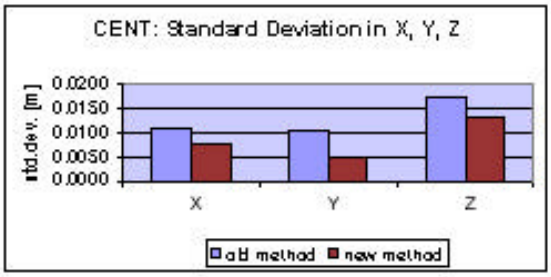

Fig. 3.11a: Standard deviations (CENT)

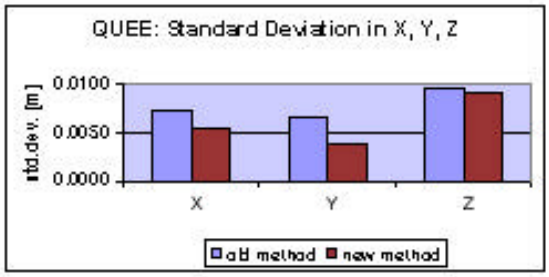

Fig. 3.11b: Standard deviations (QUEE)

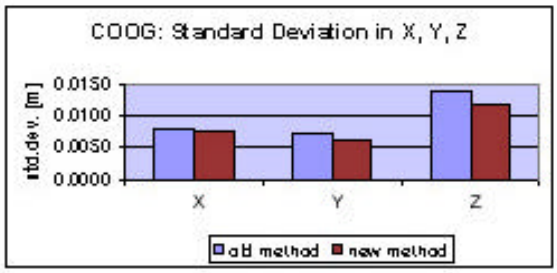

Fig. 3.11c: Standard deviations (COOG)

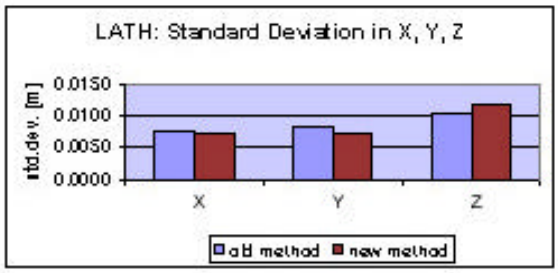

Fig. 3.11d: Standard deviations (LATH)

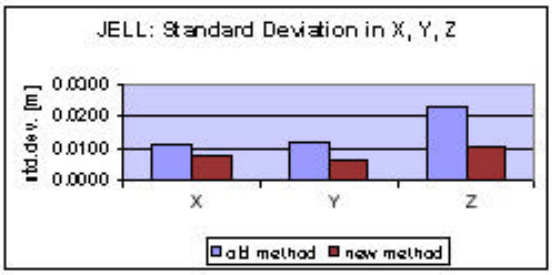

Fig. 3.11e: Standard deviations (JELL)

The reason for obtaining better coordinate results with the proposed method in spite of slightly higher RMS (or standard deviation) values of the double-differenced residuals (see Fig. 3.9) lies in the increased number of observations. If σ_{obs}^2 denotes the variance of a single observation and n is the number of observations, then the variance of the mean σ_m^2 is defined as:

$$\sigma_m^2 = \frac{\sigma_{obs}^2}{n} \tag{3-19}$$

Assuming, for example, σ_{obs} = 0.4 and n = 16 yields σ_m = 0.10, while a slightly higher standard deviation σ_{obs} of 0.5 with a larger number of double-differenced observations n = 36 results in σ_m = 0.08.

3.7 Concluding Remarks

A number of GPS deformation monitoring applications have to deal with the problem of the deforming body itself blocking out part of the sky, thereby effectively reducing the number of satellites that can be tracked by the monitoring GPS receivers. This chapter has described a method to optimise the number of double-differenced GPS observations by generating a set of independent double-differenced combinations using vector space methods, and the geometric characterisations of Boolean matrices, based on the algorithm by Saalfeld (1999).

A numerical example has demonstrated that the proposed data processing methodology does indeed improve the coordinate results. The number of double-differenced observables available to compute a solution is maximised by using all available information, thereby improving the quality of the results. A solution can be obtained even if less than four common satellites can be tracked simultaneously at all network sites. Hence the problem of the deforming body obstructing part of the sky, reducing the effectiveness of certain deformation monitoring applications, can be overcome using this data processing approach.

The benefits of processing a GPS network in multi-baseline mode as opposed to baseline-by-baseline processing, as well as the appropriate ambiguity resolution technique to be used for monitoring applications, have been discussed.